Extraordinary Hydrogen Evolution and Oxidation Reaction Activity from Carbon Nanotubes and Graphitic Carbons

Rajib Kumar Das[†], Yan Wang[†,‡], Svetlana V. Vasilyeva[†], Evan Donoghue[†], Ilaria Pucher[†], George Kamenov[§], Hai-Ping Cheng[†,‡] and Andrew G. Rinzler[†*]

[†]Department of Physics, [‡]Quantum Theory Project and [§]Department of Geological Sciences, University of Florida, Gainesville, FL 32611-8440

Supporting Information

Specially constructed Teflon electrochemical cell

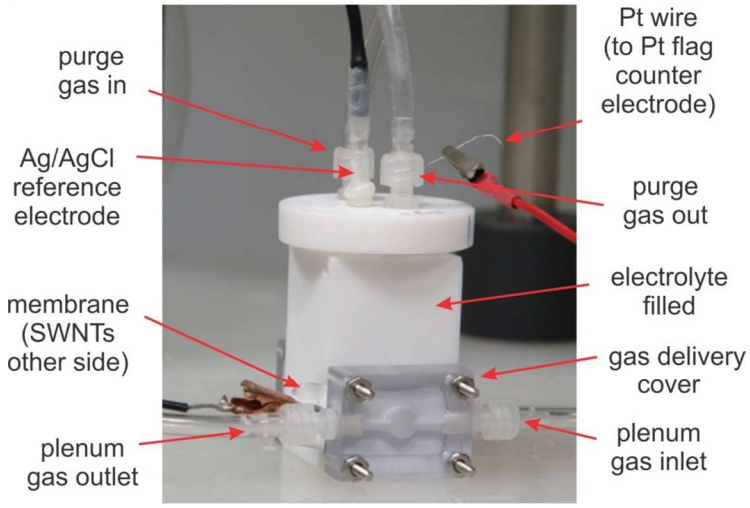

Figure S1. Photograph of the specially constructed Teflon electrochemical cell.

Rotating Ring Disk Electrode Set-up

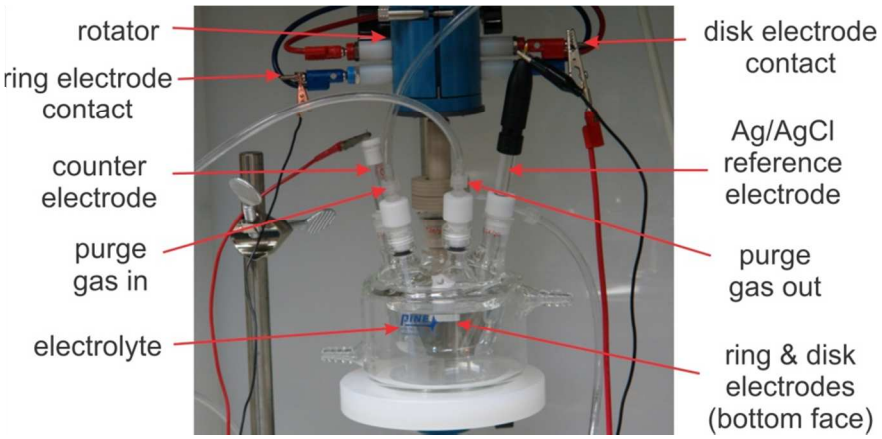

Figure S2. Photograph of the RRDE measurement set-up (Pine Instruments).

Hydrogen evolution bubbles

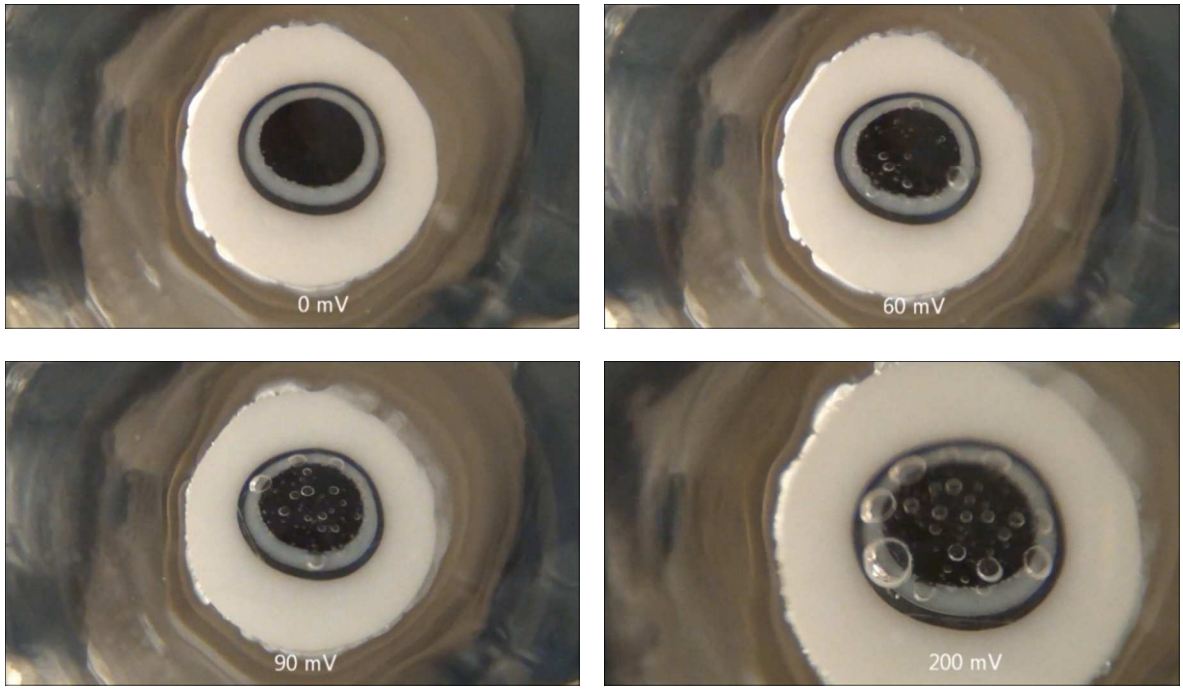

Figure S3. Hydrogen evolution bubbles from the stationary disk electrode. Shown are the ring-disk electrodes with 27 μg SWNT on the disk at the indicated potentials (*vs*. NHE) in 1 M H_2SO_4. Optical distortion of the circular electrodes occurs because of the view through the bottom of the Pyrex electrochemical cell.

HER SWNT layer RDE measurement

Figure S4. HER current from the 27 μg activated SWNTs on the glassy carbon disk electrode, measured in 1 M H_2SO_4 at 1400 rpm, scan rate 50 mV/s. The 58 mA/cm^2 current density at 200 mV overpotential yields a specific (mass basis) activity of 422 A/g. The improvement over the specific activity of 278 A/g for the measurement performed in the Teflon cell is due to the facile removal of the hydrogen bubbles created in the rotating disk measurement. These are otherwise prone to occlude electrode area in the static measurement in the Teflon cell.

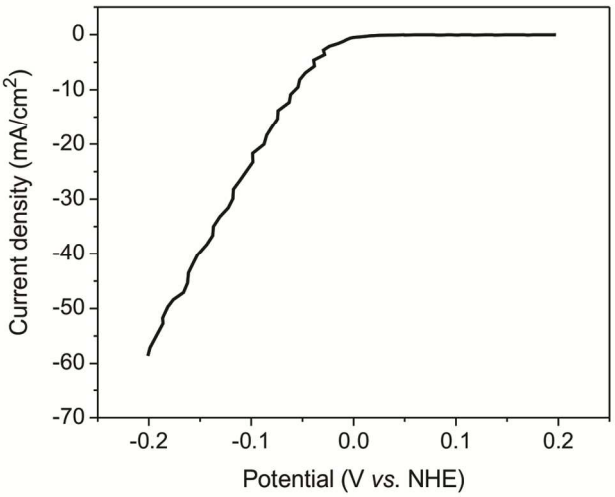

Long term measurement

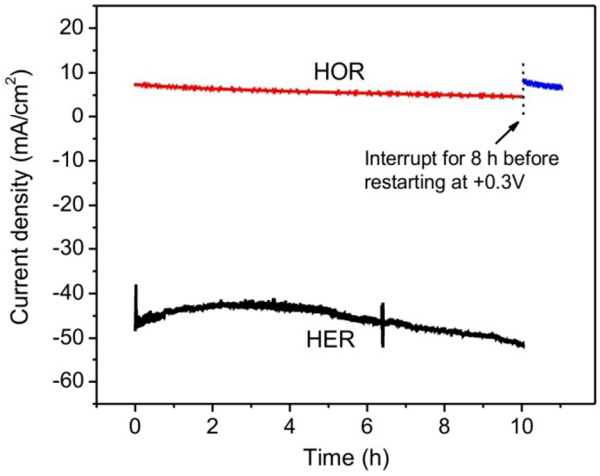

Figure S5. Extended time measurements of the HOR and HER currents for the activated SWNT film (54 μg) in the Teflon electrochemical cell in 1 M H_2SO_4 at +300 and -300 mV, respectively. The apparent slow decay observed in the HOR activity seems to be due to a confinement effect of the protons generated within the compact, tortuous path porosity of the SWNT films. When the current is interrupted, giving diffusion a chance to re-equilibrate the electrolyte concentration within the pore volumes the HOR activity returns to its original value. During the interruption the cell was decoupled from the potentiostat. The HER activity is clearly unaffected by the long term hydrogen evolution.

Near neutral pH (3 M buffer)

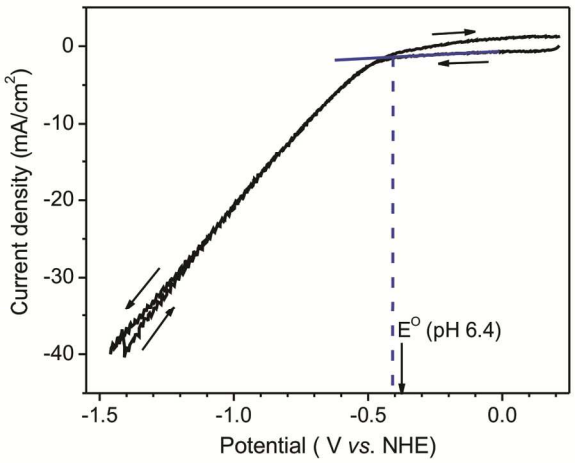

Figure S6. CV (50 mV/s scan rate) for the activated SWNT film (54 μg) in pH 6.4 buffer at a 3 M KCl concentration measured in the Teflon cell using a magnetic stir bar to stir the solution. The onset of HER occurs at ~ 30 mV overpotential. The lower onset potential compared to the 0.6 M buffer measurement discussed in the paper occurs because the higher salt concentration reduces the cell IR drop, while stirring reduces the effects of concentration polarization. What looks like increasing noise at higher currents is most likely due to a periodic disturbance by the rotating magnetic stir bar of the bubbles that form at the film surface (the "noise" stopped upon stopping the magnetic stir bar). The switch to the higher current path corresponds to a large bubble having detached from the film surface.

Seawater

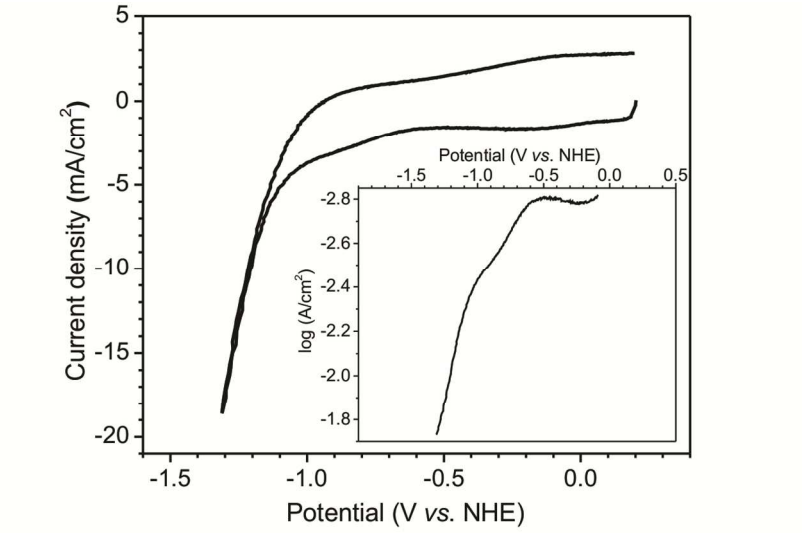

Figure S7. CV for an activated SWNT film (27 μg on the 5 mm diameter glassy carbon disk electrode, static measurement) demonstrating HER in filtered, additive free, Atlantic seawater (St. Augustine Beach, FL). The seawater was filtered through coarse paper filter. Inset shows the forward sweep with the current on a log scale to facilitate identification of the onset potential, found to be -570 mV, yielding an overpotential of ~68 mV (evaluated using the solution pH measured at the end of the sweep).

Activation in other acids

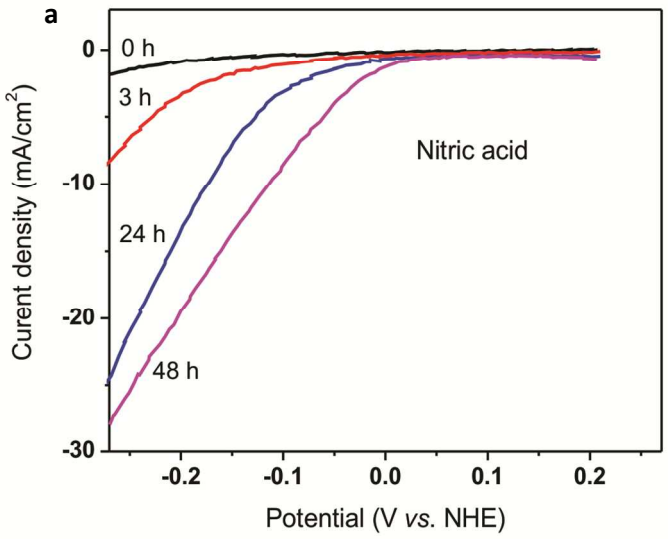

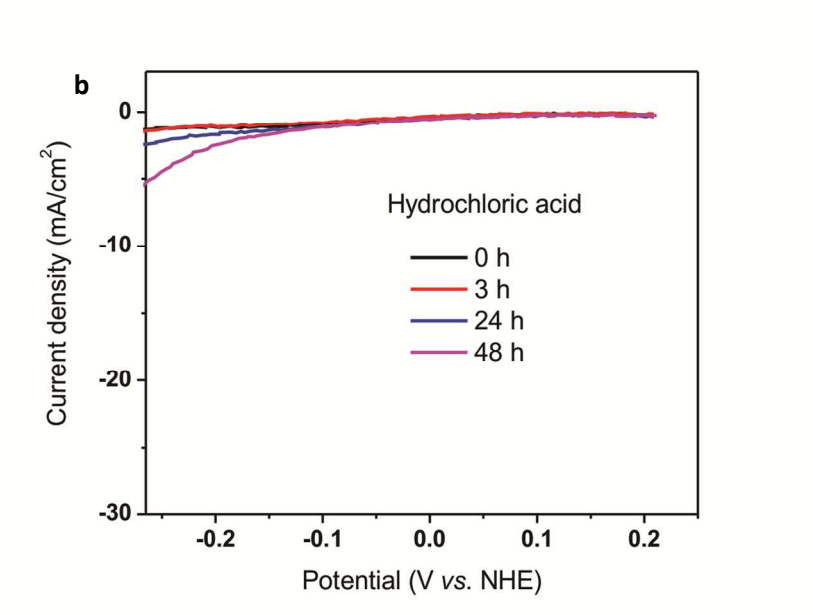

Figure S8. SWNT activation behavior in (a) 1 M nitric and (b) 1 M hydrochloric acids, respectively. HER currents measured at the indicated times.

Activation of microcrystalline graphitic rods

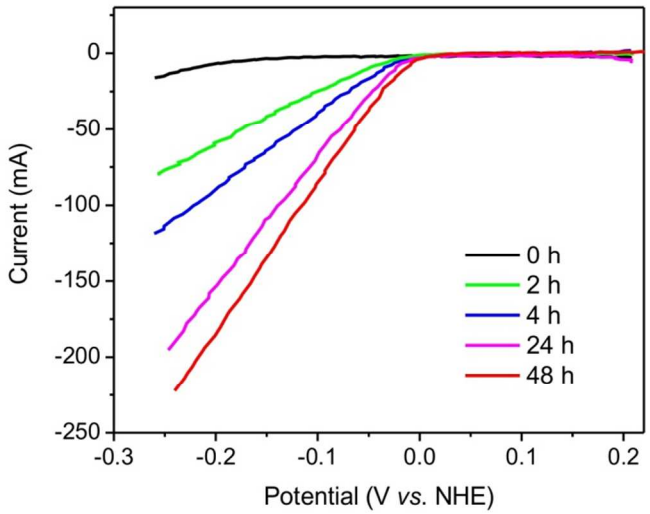

Figure S9. Evolution of the HER currents versus potential as a function of time in 1 M nitric acid for a 3.18 mm diameter graphite electrode rod (Bay Carbon).

Additional tests ruling out conventional metal catalysts

In three-terminal electrochemical measurements cathodic cycling of the working electrode implies anodic cycling of the counter electrode. Anodic cycling of platinum in acids is known to result in some degree of its corrosion. This is greatest in chlorinated acids (manuscript ref. 26) but some corrosion occurs even in sulfuric acid (manuscript ref. 27). A viable concern is that this Pt deposited onto our working electrodes during the long soaks in the acid and that this deposited Pt was responsible for the seeming activation of the carbon working electrodes. The rapid recovery of the SWNT HOR activity in the CO poisoning test (in contrast to the behavior of Pt) shown in manuscript Figure 3b provides strong evidence against such Pt contamination, but it is nevertheless prudent to have additional analyses and experiments to eliminate Pt and other metals as the source of this activity. Details and results of these follow.

HRTEM imaging

Pt (or other metal particles) deposited on the SWNTs should be visible in high resolution transmission electron microscopy (HRTEM). As noted in the manuscript our nanotube samples typically contain a small fraction of Co and Ni which are the growth catalysts used in our pulsed laser vaporization based nanotube synthesis. The major portion of these metals is removed by our purification process (2.6 M nitric acid reflux followed by cross flow filtration and a 1 h 2,700 g, low speed centrifugation). However, a fraction of the Ni and Co exist as particles protected from the acid by complete, multi-layer Fullerene shells (bucky onions) and survive this purification. The vast majority of even these particles can be removed by repeated high speed centrifugation but the high speed limits the volume of the material that can be processed. In bright-field TEM imaging all high Z metal particles will appear as dark spots. To minimize the high resolution surveys necessary to distinguish Pt that might have been deposited during the activation process we worked with a sample that had the greatest amount of the Co and Ni removed by three additional high speed centrifugations (1 h each at 23,000 g).

To prepare a thin film sample suitable for TEM imaging a very thin film (~10 nm) of the high-speed centrifuged SWNT sample was deposited onto a polycarbonate membrane (Millipore, Isopore VCTP047), which provided the support for the film during its activation in 1 M H_2SO_4 (as per the film of Figure 1a in the manuscript). After activation the film was transferred to a lacey carbon TEM grid by adhering the SWNT film side of the membrane to the grid and dissolving the polycarbonate membrane in repeated dichloromethane baths followed by methanol. Imaging was performed in a JEOL 2010F TEM. Representative images are shown in Figure S10 a-c (scale bars 200, 50 and 20 nm respectively). Improved contrast of low Z materials is attained by a slight overfocus, however this can give the illusion of high density material in spots. Zooming in revealed all of these to be low contrast and thus not Pt. All the particles seen at lower magnification were found to be empty Fullerene bucky onions upon zooming in. For

comparison we show a published TEM image of a Pt loaded GDE (20 wt%) where the 2.8 nm average diameter Pt particles are readily distinguished from the carbon.[1]

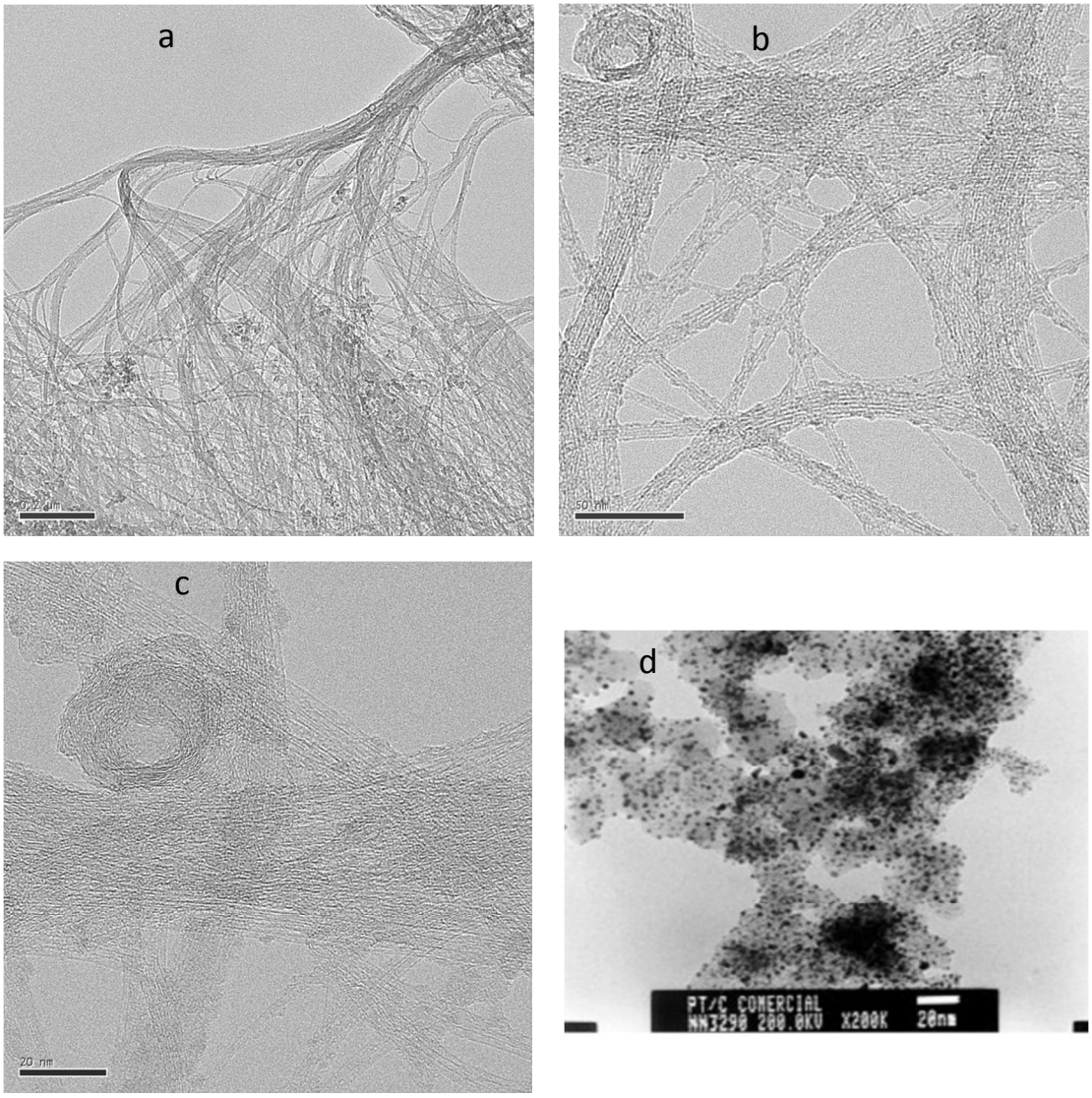

Figure S10. (a-c) HRTEM imaging of an activated SWNT film (scale bars a-200 nm, b-50 nm, c-20 nm), and (d) comparison with 20 wt% Pt loaded GDE (d-scale bar 20 nm).

Elemental analysis

Energy dispersive spectroscopy (EDS) associated with the JEOL 2010 F detected no Pt in the activated SWNT film sample; however, the sensitivity of EDS is only at the 1% level and TEM is a local technique that can probe relatively little of the sample. To perform a global survey we sent a film of our typical (low speed centrifuged) activated SWNTs, 600 nm thick, on a PTFE

membrane for proton induce X-ray emission (PIXE) analysis (Elemental Analysis, Inc. Lexington, KY). The report returns the detected elements as a mass per unit area, along with the detection limits of the measurement. PIXE is not sensitive to carbon, hydrogen or oxygen but the mass density of our films is known (manuscript ref. 12), giving ~43 $\mu g/cm^2$ of carbon for the 600 nm thick SWNT film. The PIXE scan found no trace of Pt (detection limit 0.08 $\mu g/cm^2$, 1σ confidence). As a sensitivity check the PIXE found 0.113 and 0.103 $\mu g/cm^2$ of the Co and Ni growth catalysts, respectively. These correspond to ~0.05 at% of the carbon for each metal, decreased by our typical purification from the 1 at% of each metal incorporated in the PLV target during nanotube synthesis. As noted above, electrical contact to the SWNT film on the membrane was typically made *via* a palladium contact pad sputtered across the bare membrane overlapping the edge of the SWNT film by ~2 mm. When the film was activated and measured in the Teflon cell this overlap region lay well outside the region defined by the o-ring that was electrolyte wetted and formed the electrochemically active area of the film. Nevertheless, Pd contamination of the activated area might also be of concern. The PIXE analysis also found no trace of Pd (detection limit 0.036 $\mu g/cm^2$, 1σ confidence). Pd we note would also be poisoned by CO (with even higher binding energy than Pt) in contrast to the recovery exhibited by the activated SWNTs during the CO poisoning test.

Characteristic redox peaks on Pt

Electrochemistry is a sensitive analytical technique for trace metal analysis. If Pt (or Pd) existed on the activated SWNT films we would expect to find redox peaks characteristic of Pt in CV scans. Figure S11 below shows a CV (2 mV/s) performed on a Pt electrode in oxygenated 1M nitric acid (red curve). The characteristic peaks seen on the Pt electrode are labeled. Also shown is the CV (2 mV/s) for an activated (600 nm thick) SWNT film in oxygenated 1 M nitric acid (black curve).

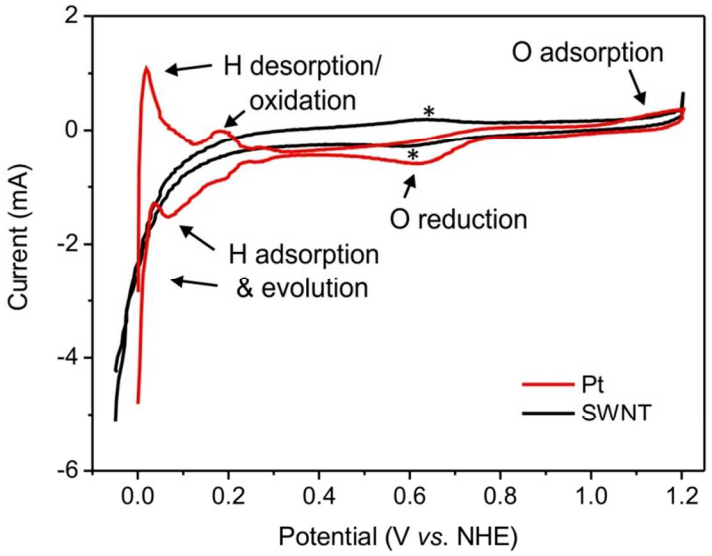

Figure S11. Redox peaks on Pt and on an activated SWNT film.

The peaks typical of Pt electrodes are simply not present in the activated SWNT film CV. The peaks in the SWNT CV labeled by asterisks are not associated with oxygen but rather reduction of quinone and oxidation of hydroquinone like groups typical of carbonaceous electrodes (manuscript ref. 1). That these latter peaks are not related to oxygen is demonstrated by a scan done in the deoxygenated acid, superimposed on the scan done in the presence of oxygen shown in Figure S12.

Figure S12. Redox peaks on an activated SWNT in 1 M HNO_3. The peak seen around 0.6 V appear whether oxygen or argon are bubbled into the electrolyte demonstrating that they are not associated with the oxygen reduction.

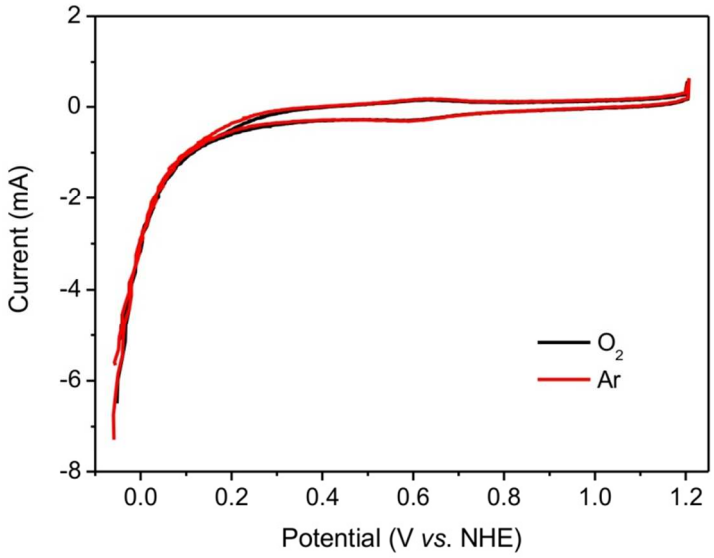

Limiting access of Pt to the SWNT electrode

To further eliminate the possibility that Pt contamination due to cycling was the source of the activity, a 500 nm thick SWNT film was activated by the cycling procedure described above but immediately after each set of 5 consecutive CV cycles the counter electrode was removed from the cell, the sulfuric acid was quickly pipette out, the cell rinsed and then refilled with fresh 1 M sulfuric acid. The film was soaked in the fresh acid for the 24 h dwell time until the rinsed Pt counter electrode was briefly replaced in the cell for the subsequent measurement and next 5 cycles. In this manner whatever trace Pt may have leached into the acid during the cycling, its access to the electrode was highly limited. Figure S13 shows the decrease in the overpotential and increased HER activity against time for this film, which is consistent, for this reduced film thickness, with the level of activation attained without such acid replacement.

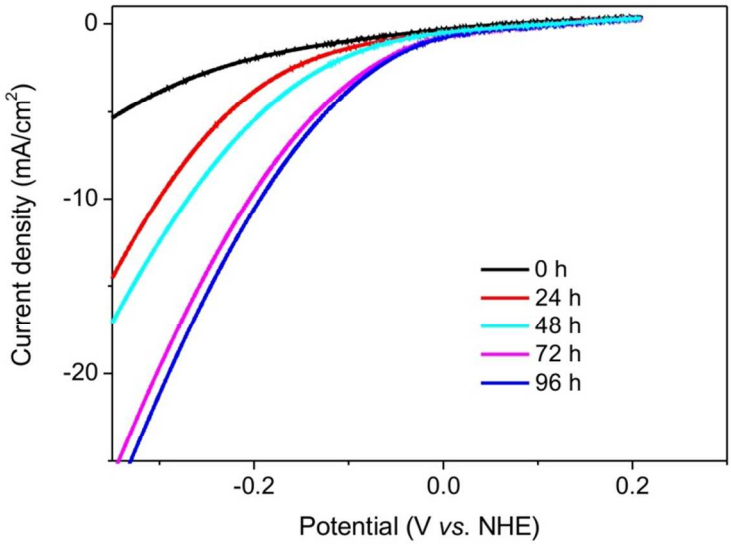

Figure S13. Voltammograms for a 500 nm thick SWNT film activation in which the Pt counter electrode shared the cell with the working electrode only during each measurement and post measurement 5 CV cycles, after which the sulfuric acid was immediately replaced with fresh acid.

Why increased accessible SWNT surface area cannot explain the observations

The overpotential is the minimum voltage necessary for the reaction to proceed for a given catalyst. Increasing the surface area at an applied voltage below that necessary for a reaction to proceed cannot increase the current from that reaction. Any multiplicative factor (reflecting an increase in the surface area) times zero remains zero. In the pre-activated SWNTs there is **no** HOR activity at any voltage, consistent with what is reported in the literature for carbons. As shown in Figure 1d, once the SWNTs are activated the reaction initiates at 0.0 V, (right where the HER reaction terminates, just as it does for the commercial Pt electrode).

Now in electrochemical measurements there are usually small currents due to impurity reactions or alternative reaction pathways (with much smaller rate constants) so it might be thought that these low level reactions are being misinterpreted as activity once the surface area increases. If that were the case we should be able to multiply the non-activated current densities by some multiplicative factor (corresponding to the multiplicative change in the surface area) and obtain curves that mimic our activated SWNT data. We do this here for the HER data shown in Figure 1a of the manuscript by applying multiplicative factors to the 0 hr current density. How large should those factors be? Statistics on the bundle diameters from AFM height measurements show the mean bundle diameter to be 5 nm which corresponds to 7 hexagonal close packed SWNTs. By what multiplicative factor does the outermost bundle area increase if the inner surface area becomes accessible? The initial bundle has circumference $\pi \cdot \mathrm{D}$, (with D = 5 nm, the bundle diameter) while the combined circumference of the 7

nanotubes is $7 \cdot \pi \cdot d$ (with the nanotube diameter d = 1.7nm, using the typical (10,10) tube diameter of 1.36 nm plus its van der Waals shell thickness of 0.34 nm) since the lengths would be the same, the factor reflecting the multiplicative change in surface area is simply $7 \cdot \pi \cdot d / \pi \cdot D = 7 \cdot d / D$ which evaluates to 2.4. This could be bigger if the bundle size were bigger so if we double the measured mean bundle diameter to 10 nm (which includes ~30 nanotubes) the area increases to a factor of $30 \cdot d / D = 30 \cdot 1.7 / 10 = 5.1$.

Figure S14 reproduces our Figure 1a from the manuscript where we also multiply the current density of the initial t = 0 hr curve, first by a factor of 10 and then by a factor of 16.5 (labeled dashed curves). These are extreme cases compared to the factors calculated above, with the latter used to match the maximum current density in our 120 h curve at -0.24 V. Note the completely different character of these curves from the fully activated curves (96 or 120 h curves) for which the overpotential (knee in the curves) has shifted to 0.0 V. There is simply no way that the dramatic change in the overpotential observed can be attributed to an increase in the surface areas (even for the greatly exaggerated factor of 16.5 corresponding to more than 3 times the upper bound of 5.1 for the change in surface area in going from 10 nm diameter bundles to fully accessible, individual nanotubes).

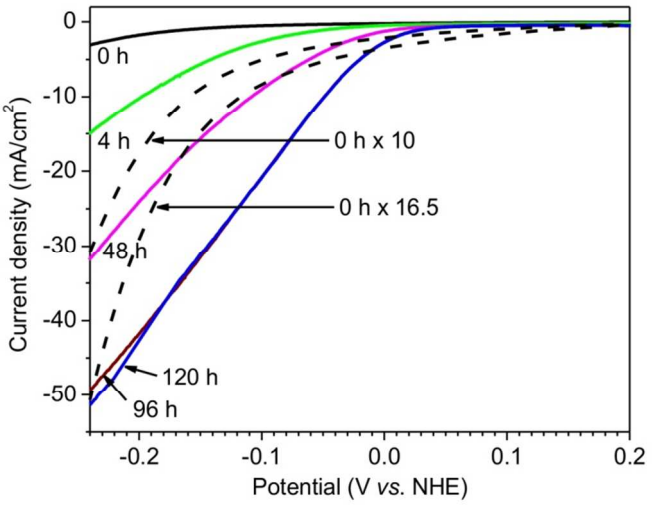

Figure S14. Figure 1a from the manuscript with the 0 h curve multiplied by a factor of 10 and 16.5 (dashed lines as labeled) to mimic the result of increased currents from an increased surface area.

First-principles density-functional-theory (DFT) calculations

First-principles calculations were performed using density functional theory implemented in the plane-wave-basis-set Vienna *ab initio* simulation package (VASP).[2] A (10,10) armchair SWNT was used in simulating the Volmer, Tafel, and Heyrovsky reactions; four primitive unit cells (160 C atoms per supercell) were used to minimize the interaction among the adsorbates along the nanotube axis. The metallic (10,10) nanotube was modeled because its diameter is that of the average nanotube diameter for the material used in the experiments. For the semiconducting nanotubes in the material, once electrons are added their Fermi level shifts into the conduction band and we anticipate behavior equivalent to that of the metallic nanotube modeled. For the

adjacent Tafel reaction two (10, 10) armchair nanotubes were used aligned parallel to each other, with two primitive unit cells for each nanotube and a tube-tube wall separation of 3.7 Å. This tube-tube wall distance is larger than the typical non-intercalated 3.4 Å to allow for an intercalant (some distance away) causing such local separation. A one-dimensional periodic boundary condition was applied along the nanotube axis with a 3 k-point sampling for the Volmer, Tafel (same nanotube) and Heyrovsky reactions, and a 6 k-point sampling for the adjacent Tafel reaction. A large vacuum spacing of 15 Å between two images along directions perpendicular to the nanotube axis is used to prevent interaction between adjacent images. Relaxation of H, H_2, H_2O and the carbon atoms of the SWNT close to the reaction center was allowed. For the adjacent Tafel reaction in the graphite systems a 6 x 6 AB-stacked bulk supercell and a 2 x 2 x 3 k-point sampling were used, and the interlayer distances were fixed at 5 Å. Relaxation of H, H_2 and the carbon atoms of the graphite close to the reaction center was allowed.

All geometries were optimized until the forces on atoms fell below the convergence criterion of 0.02 eV/Å. Projector augmented wave potentials with kinetic energy cutoff of 400 eV were employed in all simulations. Exchange and correlation functionals were described within Perdew-Burke-Ernzerh generalized gradient approximation.[3] Minimum energy pathways and the reaction barriers were calculated by using the climbing-image nudged elastic band method.[4] The effect of van der Waals interactions was taken into account by using the empirical correction scheme.[5]

To simulate the applied electrochemical potential, modeling was performed with increasing excess electrons on the nanotube(s). Such excess electrons are driven onto the nanotubes by the applied potential due to non-Faradaic charging in the electrolyte (conversion of protons to H_2 is Faradaic, taking away two electrons per molecule evolved, but the high conductivity of the nanotubes rapidly replenishes electrons as they are removed, leaving the nanotube in a charge state consistent with the applied potential). Because of the nanotube low density of electronic states their non-Faradaic charging is limited by the quantum capacitance to ~1 fF/μm of nanotube length.[6] This corresponds to 6.3 excess electrons per nanometer (160 carbon atoms for a (10,10) SWNT) per applied volt for a single nanotube surrounded *on all sides by electrolyte*. Taking the SWNT charge neutrality level as -4.6 eV with respect to vacuum[7] this means that 0 V with respect to NHE (-4.4 eV) corresponds to +0.2 V relative to charge neutrality, inducing ~1.3 excess electrons/nm of tube length. Three excess electrons are obtained at ~0.27 V with respect to NHE. We accordingly model the case of a nanotube having zero, one and three excess electrons per nanometer of tube length (160 carbon atoms). The reaction barriers obtained are not expected to have sufficient quantitative correspondence with experiment to permit their use in *e.g.* predicting measured currents. We rather pay attention to trends and relative barrier heights.

Volmer reaction

Figure S15a-c (next page) shows steps along the reaction between a (10, 10) SWNT (160 carbon atoms per supercell) and a hydronium ion surrounded by three H_2O molecules leaving a hydrogen atom chemisorbed to the SWNT. The initial structure of these molecules is taken from Hodges *et al.* (manuscript ref. 30). Figure S15d shows the calculated activation barrier for the Volmer reaction for a neutral and charged nanotube. Both the reaction barrier and the final energy decrease relative to the initial state with increasing charge on the tube. For the neutral SWNT the activation barrier is 1.22 eV, but for a 3e/160C charged SWNT the barrier is reduced to 0.44 eV.

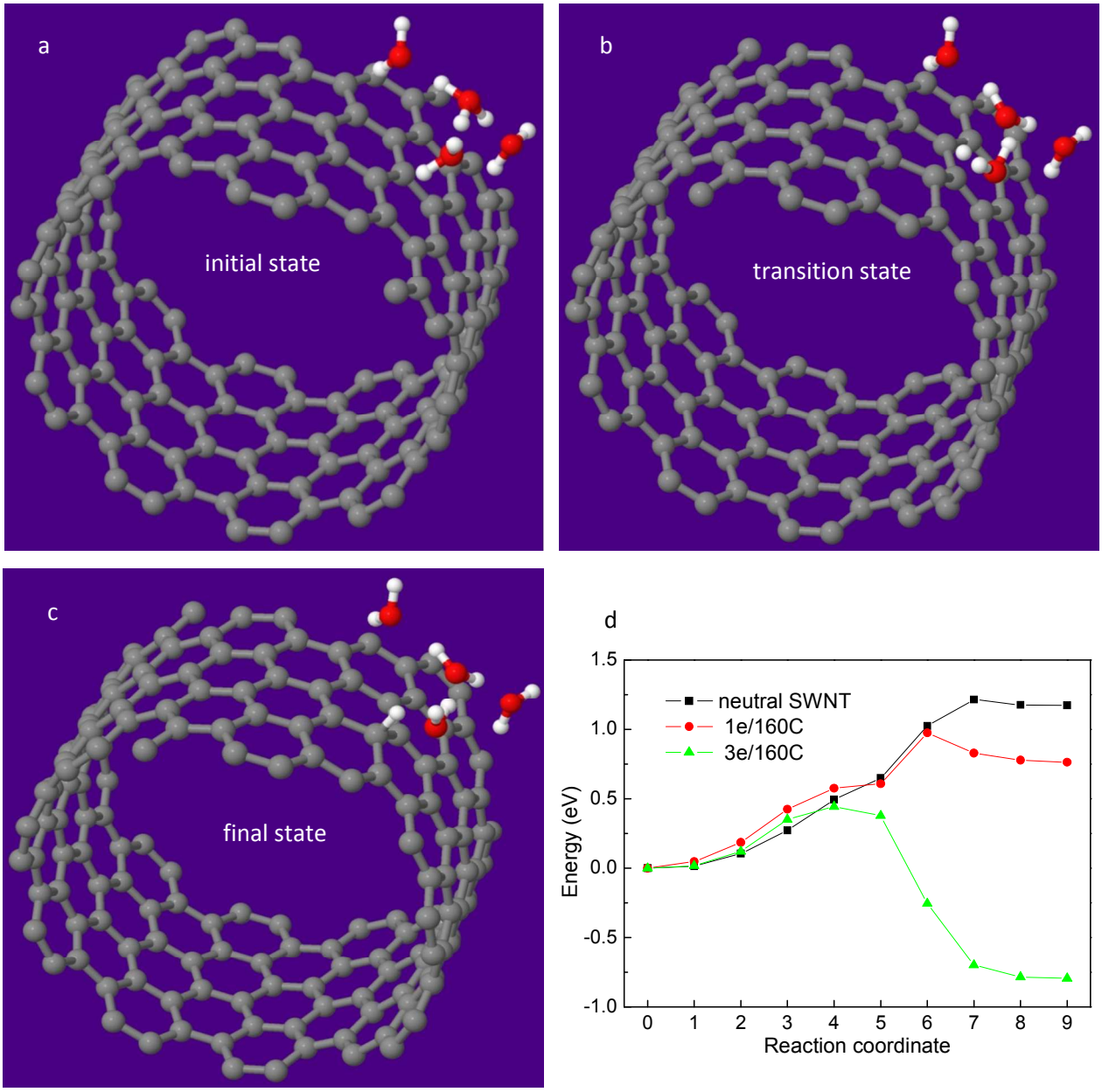

Figure S15. Volmer reaction. a. Initial state. A Hydronium ion surrounded by three hydrogen bonded water molecules is physisorbed to the surface of a (10,10) SWNT. b. Transition state with the proton moving to the SWNT. c. The final chemisorbed state. The proton is (mostly) discharged in the process acquiring ~0.9e from the SWNT. d. Calculated minimum energy pathway. Energy values are evaluated with respect to the corresponding initial state. The images are produced using the Jmol package.[8]

Tafel reaction (same nanotube)

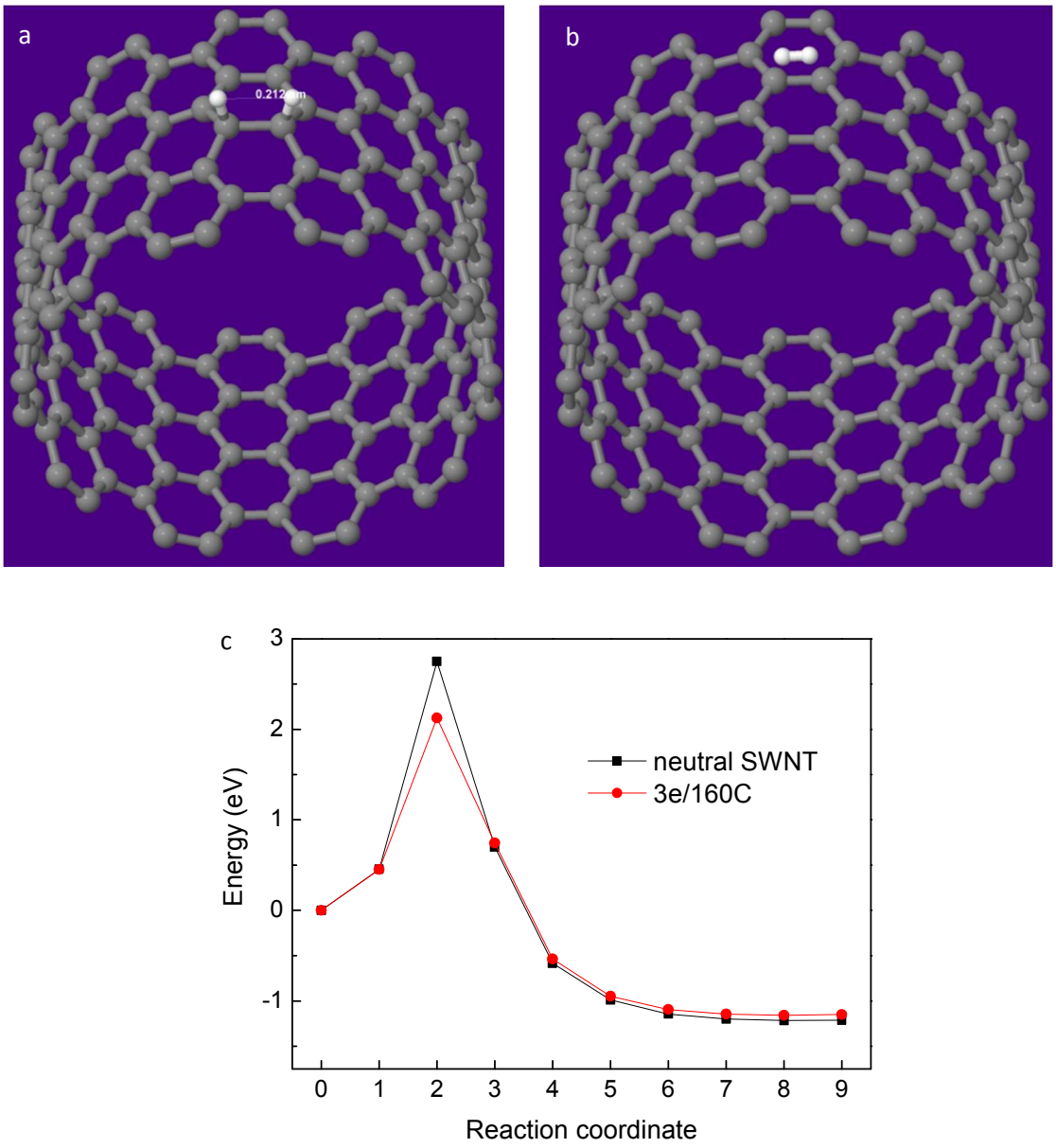

Figure S16. a. Two hydrogen atoms chemisorbed onto the same SWNT at a nearest neighbor site. b. The final desorbed state. c. Calculated minimum energy pathway. The reaction barrier is large and remained large even for the case of the charged nanotube. Also considered were the cases of the chemisorbed hydrogen atoms occupying the 2nd and 3rd nearest neighbor sites. They too gave large barriers to the reaction with the barriers remaining large upon charging the SWNT. Our results for the neutral nanotube with the hydrogen atoms occupying the 1st, 2nd and 3rd nearest neighbor sites, were consistent with those obtained by Zhang *et al.* for a pure (8, 0) SWNT,[9] who considered hydrogen evolution (release) in the context of hydrogen storage.

Adjacent Tafel reaction (SWNTs)

Figure 5 of the manuscript shows hydrogen atoms chemisorbed to adjacent nanotubes, in close proximity, evolving off as a hydrogen molecule. As shown in Figure S17 the reaction barrier depends on the initial proximity of the chemisorbed hydrogen atoms. For initial hydrogen separations of 2.64 Å (Figure S17a) and 2.28 Å (Figure S17b), the activation barriers for the adjacent Tafel reaction are 0.89 eV and 0.60 eV, respectively. At still smaller hydrogen separation the activation barrier is further reduced. For a separation of 1.47 Å, as shown in Figure S17c, there is no activation barrier for the reaction. As for the Tafel reaction occurring on the same nanotube, charging the two nanotubes had only a minor effect on the calculated activation barrier for the reaction.

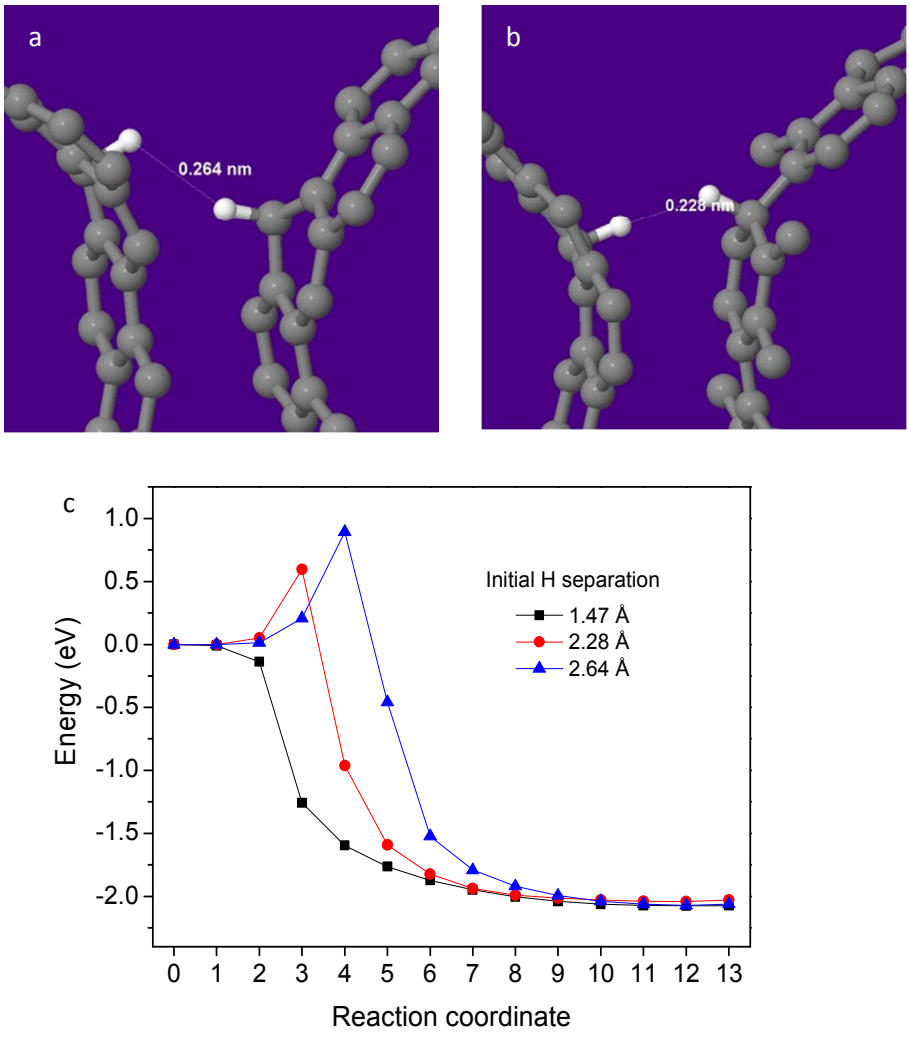

Figure S17. Adjacent Tafel reaction. a. Two hydrogen atoms (chemisorbed to two SWNTs) at initial separation of 2.64 Å. b. Two hydrogen atoms at initial separation of 2.28 Å. c. Calculated minimum energy pathway for the reaction.

Heyrovsky reaction

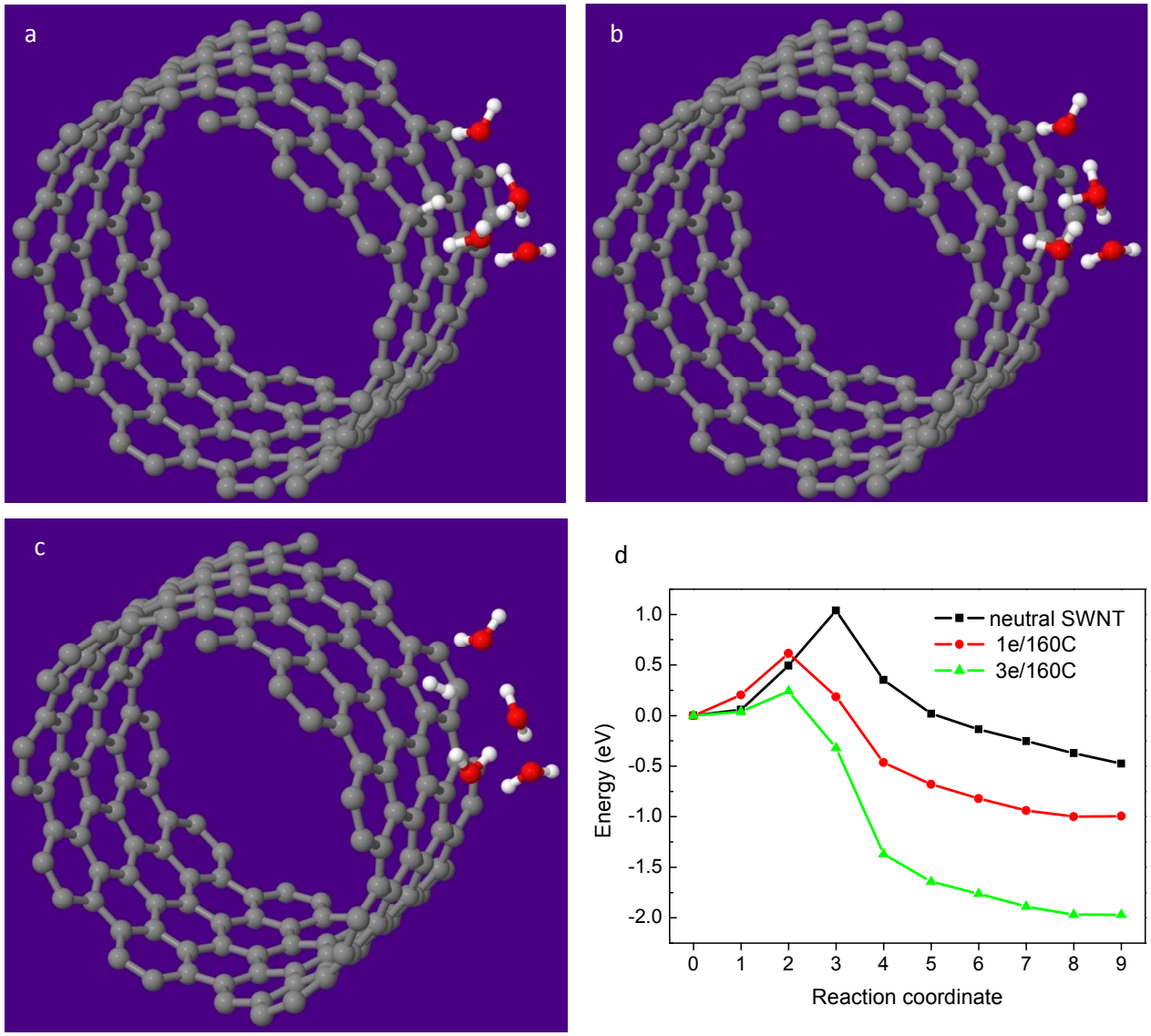

Figure S18. Heyrovsky reaction. a. The initial state consisting of a hydrogen atom chemisorbed to a SWNT and a nearby hydronium ion with three associated water molecules. b. A transition state in which the nanotube chemisorbed hydrogen is attracted to the nearest hydrogen of the hydronium ion. c. The final state in which the hydrogen atoms have become H_2 and the hydronium a water molecule. d. Calculated minimum energy pathway of the reaction for the case of a neutral SWNT and a nanotube with an excess charge of one and three electrons per 160 carbon atoms. The reaction barrier decreases dramatically with the charge state of the SWNT. The neutral SWNT results an activation barrier of 1.04 eV, but for a charge of 3e/160C the barrier is reduced to 0.24 eV.

Adjacent Tafel reaction (graphite)

Figure S19 shows the adjacent Tafel reaction for an AB-stacked bulk graphite. Again, the reaction barrier depends on the initial proximity of the hydrogens. In Figures S19a-c they lie along a vertical line but one H atom may be offset laterally with respect to the other. The greater their initial separation the larger the reaction barrier. As shown in Figure S19d for an initial H separation of 2.17 Å the calculated activation barrier is 0.27 eV. For a separation of 1.58 Å there is no activation barrier for the adjacent Tafel reaction.

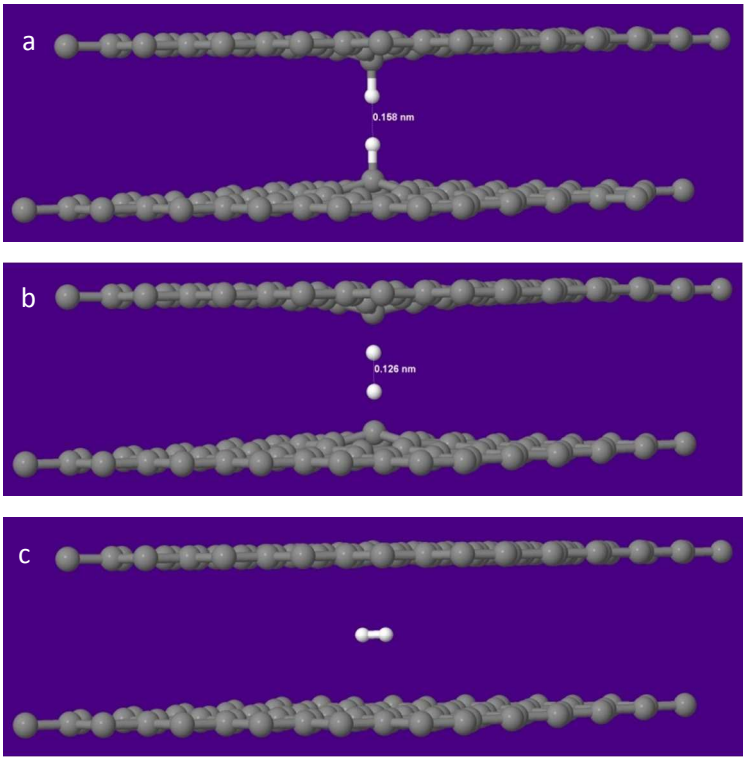

Figure S19. Adjacent Tafel reaction for graphite. Sheet separation 5 Å (assumes a near lying intercalant inducing this local separation). a. The initial state. b. Transition state. c. Physisorbed state. d. Calculated minimum energy pathway for two initial H atom separations. The reaction barrier depends on the initial proximity of the hydrogens.

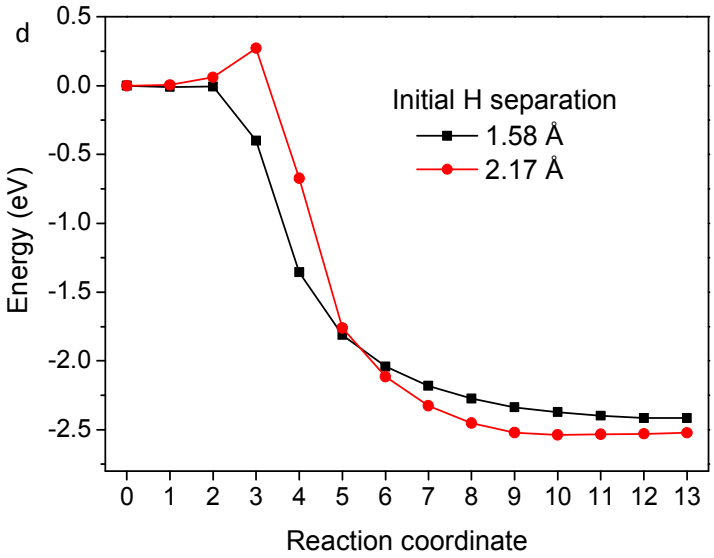

Movie

The movie file "Movie Rods-HER-at-90-200-400mV" shows HER from two Bay Carbon graphite rods one previously activated (right) and the other not (left) in 1 M nitric acid. The two rods are electrically connected (in parallel) as the working electrodes and driven at sequentially 90, 200 and 400 mV overpotential. HER bubbles are seen immediately from the activated rod while the non-activated rod only begins to exhibit H_2 bubbles at the greatest overpotential.

Supporting Information references

1. Reprinted from J. Power Sources, Vol. 169, Issue 1, Chaparro, A. M.; Benítez, R.; Gubler, L.; Scherer, G. G.; Daza, L. Study of Membrane Electrode Assemblies for PEMFC, With Cathodes Prepared by the Electrospray Method, 77-84, Copyright (2007), with permission from Elsevier.

2. Kresse G.; Furthmüller, J. Efficiency of Ab-Initio Total Energy Calculations for Metals and Semiconductors Using a Plane-Wave Basis Set, *Comput. Mat. Sci.* **1996**, *6*, 15-50.

3. Perdew, J. P.; Burke, K.; Ernzerhof, M. Generalized Gradient Approximation Made Simple, *Phys. Rev. Lett.* **1996**, *77*, 3865-3868.

4. Henkelman, G.; Uberuaga, B. P.; Jónsson, H. A Climbing Image Nudged Elastic Band Method for Finding Saddle Points and Minimum Energy Paths, *J. Chem. Phys,* **2000***, 113*, 9901-9904.

5. Grimme, S. Semiempirical GGA-Type Density Functional Constructed With a Long-Range Dispersion Correction, *J. Comput. Chem.* **2006**, *27*, 1787-1799.

6. Heller, I.; Kong, J.; Williams, K. A; Dekker, C.; Lemay, S. G. Electrochemistry at Single Walled Carbon Nanotubes, *J. Am. Chem. Soc.* **2006**, *128*, 7353–7359.

7. Zhao, J.; Han, J.; Lu, J. P. Work Functions of Pristine and Alkali-Metal Intercalated Carbon Nanotubes and Bundles, *Phys. Rev. B* **2002**, *65*, 193401-1-4.

8. Jmol: An Open-Source Java Viewer for Chemical Structures in 3D. http://www.jmol.org/

9. Zhang, Z.; Cho, K. *Ab Initio* Study of Hydrogen Interaction With Pure and Nitrogen-Doped Carbon Nanotubes, *Phys. Rev. B* **2007**, *75*, 075420-1-6.